doi:10.2489/jswc.74.1.1

Delineation of tile-drain networks using thermal and multispectral imagery—Implications for water quantity and quality differences from paired edge-of-field sites

T.N. Williamson, E.G. Dobrowolski, S.M. Meyer, J.W. Frey, and B.J. Allred

Abstract: As part of the Great Lakes Restoration Initiative, paired edge-of-field sites were established in high priority subwatersheds to assess the effectiveness of agricultural management practices. One pairing was in Black Creek, a tributary to the Maumee River and Lake Erie. These fields were paired because of similarity in soils, topography, and agricultural management. Following two years of baseline data collection from these fields, consistent differences in water quantity and quality were observed for tile networks draining the fields, despite these fields being adjacent and managed together. Consequently, it was hypothesized that differences in subsurface water movement, specifically tile-drain density and connectivity, were the source of the observed differences. Our objective was to map the tile-drain network using remote sensing methodology in order to improve the understanding of nutrient and water transport as well as management on these fields. A combination of multispectral and thermal imagery, collected in spring of 2017, was incorporated to delineate the tile-drain network within each field. This imagery led to locating a cracked tile, which provided a direct path for overland flow to enter the tile-drain system and suggested that a tile-drain segment under the road connected the two fields. A ground-penetrating radar survey verified multiple tile locations, including the tile segment under the road. The distribution of these tiles helps explain the difference in water quantity and quality in the two fields.

Key words: edge-of-field—Great Lakes—nutrient management—tile drains—unmanned aerial systems—water quality

The Great Lakes Restoration Initiative (GLRI) began in 2010, with the goal of restoring and protecting this freshwater resource as well as the surrounding coastline (USGS 2016). Nearshore health and nonpoint source pollution was identified as one focus, with the goal of protecting drinking water and recreation, especially along the nearshore waters that are less than 30 m deep. Most of Lake Erie falls into this nearshore category, including the area near the Maumee River outlet. Potentially harmful algal blooms (HABs) reached a historic level in 2014 where the Maumee River discharges into Lake Erie, affecting drinking water intakes and limiting use of both the river and lake. While the cause of HABs is complex, nutrient loading is considered a key mechanism in triggering and sustaining these conditions (Ho and Michalak 2015).

Excessive runoff from row crop agriculture has been identified as an important source of nutrient loading associated with HABs, specifically nitrogen (N) and phosphorus (P) that are applied in order to boost crop production. General decreases in annual loads of total P (TP) have been tied to improvements in point-source management. However, the contribution from nonpoint sources, including agricultural runoff, is delivered to the lake from tributaries and averages 71% of the annual total (Maccoux et al. 2016). There is high interannual variability in nonpoint sources, partially as a function of land management, but also as a function of climatic variability—year to year differences in growing conditions and precipitation patterns. Higher precipitation and discharge result in increased P and N loads from nonpoint sources. High precipitation years, when timing of fertilizer application to fields is difficult to plan, are periods when field management of surface runoff and soil water is key to minimizing nutrient concentrations in streams and water bodies (Stuntebeck et al. 2011).

Historically, tile drains have been installed into agricultural fields as a water-management technique to assist with the drainage of excess water from the soil to improve crop yields (Gökkaya et al. 2017). Subsurface tile-drain laterals are typically installed between depths of 0.75 to 1 m below the ground surface, spaced 5 to 25 m apart (Zucker and Brown 1998), and delivered to streams by main lines that are typically wider in diameter and deeper in the soil. In the midwestern region of the United States (Midwest), various patterns of tile-drain networks (e.g., random, parallel, and herringbone) are common configurations (Zucker and Brown 1998).

Tile-drain networks accelerate water removal from poorly drained soils developed on glacial till and lakebed deposits where surface slope is <5%, improving yields (Fausey et al. 1995) and enabling earlier access to fields after storms, which is especially critical in the spring for planting and adding fertilizer and pesticides. However, one unintended consequence of these tile drains is the bypassing of beneficial conservation practices and direct transport of nutrients to streams. Tile drains act as pathways for both dissolved nutrient forms, such as nitrate (NO_3) (Baker et al. 2006) and orthophosphate (PO_4^{3-}; Smith et al. 2015), as well as particulate forms of N (Cuadra and Vidon 2011) and P that travel via macropores through the soil profile (Gentry et al. 2007; Vidon and Cuadra 2010). Tile drains with a direct connection to the surface exhibit a different physical and chemical signature, specifically, the consistent

Tanja N. Williamson (corresponding author) is a research hydrologist-pedologist with the Ohio-Kentucky-Indiana Water Science Center, US Geological Survey (OH-KY-IN WSC, USGS), Louisville, Kentucky. **Edward G. Dobrowolski** is a hydrologist in Indianapolis, Indiana, and **Shawn M. Meyer** is a hydrologic technician in Louisville, Kentucky, for the OH-KY-IN WSC. **Jeffrey W. Frey** is a supervisory hydrologist and deputy director in Indianapolis, Indiana, for the OH-KY-IN WSC. **Barry J. Allred** is a research agricultural engineer with the USDA Agricultural Research Service (ARS) Soil Drainage Unit in Columbus, Ohio.

transport of suspended sediment in conjunction with higher concentrations of total N and P (Capel et al. 2018).

While relations between tile drainage and nutrient transport have been studied, there are complications to developing uniform management guidelines that maximize the benefits of tile drains while minimizing the pitfalls. One limitation is that the extent, connectivity, and density of tile drains are commonly unknown because local networks are installed and managed independently and are frequently a mix of materials, design, and age. Locating and mapping tile-drain networks through conventional (manual) ground-truthing techniques is labor intensive and time consuming, especially when attempting to map large fields or drainage basins (Gökkaya et al. 2017). Integration of aerial photography and other remote sensing technology with geospatial analysis has been used to assist with locating tile-drain networks in agricultural fields (Zucker and Brown 1998). However, geospatial analyses based on soil properties, topography, and land management result in different areas being identified as tile-drained relative to satellite and aerial photography surveys (Naz et al. 2009; Gökkaya et al. 2017), suggesting that a better understanding of which type of imagery and the timing of that imagery may increase success. Small-area remote sensing approaches are a good way to compare different techniques that are transferable to regional inventories. However, these attempts have not been universally successful, and more needs to be known about the best combination of imagery type, along with environmental and field conditions and tile characteristics that reliably discern tile-drain networks. For example, near-infrared imagery flown by plane after rainfall and harvest did not detect any known tiles in fields with conservation tillage, but did effectively delineate known tiles in traditionally tilled fields (personal communication, Nancy T. Baker, US Geological Survey [USGS], November of 2005).

Our objectives were to (1) document the location, density, and connectivity of tiles for paired fields that are being monitored at the outlet of topographically enclosed agricultural areas (known as edge-of-field sites); (2) explain the differences in water quantity and water quality between these paired fields that share the same soil, topographic, and agricultural management characteristics; and (3) identify a data-collection technique that could be extended to other locations where the tile-drain distribution is not known. After two years of data collection, consistent differences in water quantity and quality were observed for tile-drain networks at these paired edge-of-field sites, despite the close proximity and identical management. Since other environmental aspects were similar between the two fields, our hypothesis was that a difference in the tile-drain network was the reason for observed differences.

Materials and Methods

Site Description. These paired fields are one of several GLRI edge-of-field monitoring sites selected to focus on subcatchments of basins identified as having high P loads (Robertson and Saad 2011), with the goal of quantifying the effect of individual management practices on nutrient and sediment transport. The concept behind these sites is that, after a baseline data collection period, one field will be targeted with specific agricultural management practices while the other field is maintained as a control. This site is in northeastern Allen County, Indiana, within the Black Creek watershed—a 50 km^2 tributary basin of the Maumee River. Land use in the Black Creek basin is 73% agricultural, primarily row crops consisting of corn (*Zea mays* L.) and soybeans (*Glycine max* L.), with relatively equal areas of rural development (7.5%) and natural vegetation (forest, prairie, shrub, and wetland; 6.4%) (Homer et al. 2012). Approximately 13% of this basin is pasture, most of which sustains horses. Soil series were acquired from the Soil Survey Geographic database using Web Soil Survey (USDA NRCS 2016). Reaches of Black Creek and minor contributing tributaries in the Black Creek watershed have been identified as impaired for nutrients, biological communities, and *E. coli* for the Clean Water Act (USEPA 1972) for section 303d (IDEM 2016).

Water Quantity and Quality Monitoring. The Indiana edge-of-field site consists of two adjacent agricultural fields separated by a north-south running road. The western field is 16.8 ha (Indiana Office of Information Technology 2012) of a 25.3 ha area monitored by the surface flume—the remaining area is forest. The eastern field is 14.2 ha of a 14.5 ha area, which also includes a homestead. These tile-drain networks are subsurface only, with no managed surface openings. The two years of data presented in figures 1 and 2 are from the baseline period for these fields (September 29, 2015, to September 30, 2017). Each field is monitored by separate surface-runoff and tile-drain flumes to measure discharge and sample water quality (table 1); surface and tile-drain flumes are collocated with the intention of sampling the same total area. Automatic sample collection is facilitated by a combination of timed and manual triggering both during storms and under low-flow recession periods between events. Water quality samples were analyzed at the Water and Environmental Analysis Laboratory, University of Wisconsin–Stevens Point, using standard methods (Stuntebeck et al. 2008) for concentrations of individual N components, which are summed as total N (TN), total and dissolved P (PO_4^{3-}), and suspended sediment (SSC). Data are available on the National Water Information System (NWIS) Web interface (USGS 2017). Meteorological data, collected at the flumes of the western edge-of-field site, include air and soil temperatures, precipitation, soil-water content, and solar radiation. Methods and equipment for these sites are similar to those described by Stuntebeck et al. (2008), with the exception that no crest-stage gages were used at these sites. Monitoring began on September 29, 2015. Soil sensors were calibrated at the beginning of the study, but left undisturbed after that. Discharge and water quality data were downloaded from NWIS on December 22, 2017, and aggregated in R (R Core Team 2014) and R-Studio, using packages dataRetrieval (Hirsch et al. 2017), hydroTSM (Zambrano-Bigiarini 2017), and swmrGraphs (Lorenz 2015). Precipitation is published on NWIS as part of USGS Site ID 411228084541701. Other meteorological data can be accessed through NWIS and are preliminary.

Collection and Processing of Multispectral and Thermal Infrared Imagery. Remote sensing data were collected during two separate periods in spring of 2017: April 18 and May 9 to 10. Both fields were relatively bare, with corn residue. The April trip had been planned to gather baseline imagery for the site after a day of rainfall (April 15). The May trip was planned in response to a large event—10 days of intermittent rain. Cameras attached to a gimbal (FLIR Systems, Wilsonville, Oregon) or a static mount (MicaSense, Seattle, Washington) were sus-

Figure 1
Daily mean and cumulative discharge. The smaller field (East) produced a similar volume of surface discharge to that from the larger field (West). The eastern tile-drain network produced discharge after more events, for a longer duration, and with a higher total than the western tile-drain network. Area-normalized discharge averaged over the two years of data collection was 1,344 m^3 ha^{-1} y^{-1} from the western field, 1,989 m^3 ha^{-1} y^{-1} from the eastern field, 985 m^3 ha^{-1} y^{-1} from the western tile network, and 1,868 m^3 ha^{-1} y^{-1} from the eastern tile network.

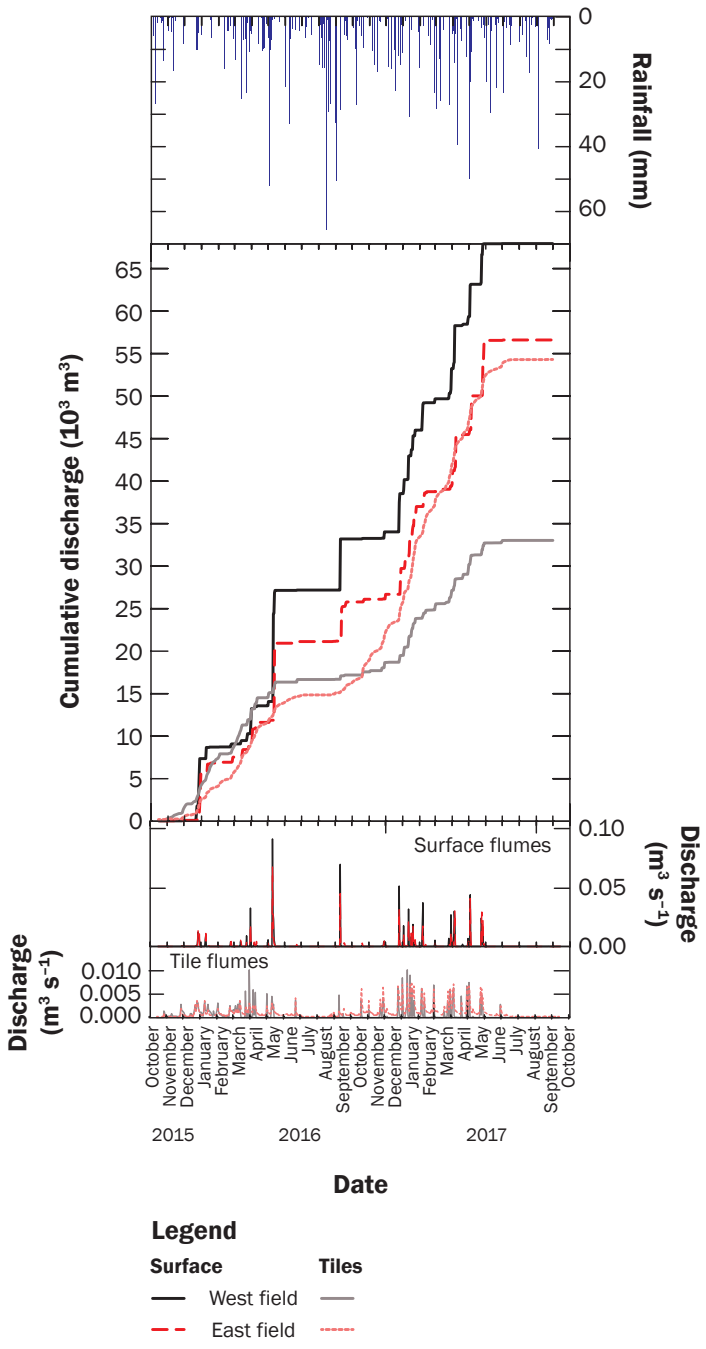

pended from a 3DR Solo quadcopter (3DR Inc., Berkeley, California) and flown at 92 m above ground level; each camera was flown separately. Multispectral data were collected using a MicaSense RedEdge camera with 75% overlap (both along the flight line and between parallel flight lines) at a speed of 7 m s^{-1} with a two second interval for image collection that included geo-referenced images. Multispectral image collection was done during daylight hours—approximately 10 a.m. to 3 p.m.—on both April 18 and May 10. This multispectral camera provides independent images for five wavelength ranges that are co-located and processed together: blue (B; approximately 475 to 500 nanometers [nm]), green (G; 550 to 560 nm), red (R: 660 to 670 nm), red-edge (710 to 720 nm), and near infrared (NIR; 820 to 860 nm) (MicaSense Inc. 2015). Images are provided as R-G-B and as NIR-B-G. Multispectral imagery had a 6-cm ground resolution. Thermal-infrared data were collected using a FLIR Vue Pro R 640 camera with an uncooled vanadium oxide microbolometer and a 13 mm lens attached to an OEM gimbal specific to the 3DR Solo. Thermal images were collected using at least 65% flight-line overlap and 55% sidelap at a speed of 5 m s^{-1}. These images were also collected in two second intervals and geo-referenced after collection by integrating the flight logs and photo timestamps using GeoSetter (3.4 BETA; Friedemann Schmidt, Berlin, Germany). The FLIR Vue Pro R is radiometrically calibrated, so the 16-bit data (DN) were converted to temperature as

$$\text{degrees Celsius} = 0.04 \times \text{TIR} - 273.15 \quad \text{(PIX4D 2018)}, \qquad (1)$$

in order to provide an approximate ground temperature, where TIR is the thermal infrared radiation recorded by the camera. Thermal imagery had an 11-cm ground resolution. Thermal images were collected during either the early morning (7 a.m. to 10 a.m. on May 10) or late afternoon (3 p.m. to 5 p.m. on May 9 and 10). The May of 2017 data acquisition, which used both cameras, required approximately 15 hours in the field. All images were processed in Photoscan (1.3.3; 1.3.4; Agisoft LLC, St. Petersburg, Russia). Multispectral and thermal-infrared imagery and point cloud data are available through a USGS data release (Williamson and Meyer 2018).

Collection and Processing of Ground Penetrating Radar Data. In order to verify interpretation of the multispectral and thermal imagery, 11 ground penetrating radar (GPR) transects, totaling 6,185 m, were traversed on December 13, 2017. A Sensors and Software Inc. (Mississauga, Ontario, Canada) Noggin GPR system with 250 MHz (cen-

Figure 2
Boxplots of water quality. Date of occurrence of maximum concentrations are noted for each component. Note that concentrations from the western tile network are more similar to the surface water concentrations than to the eastern tile network. The same number of samples (shown in 2a) were analyzed for each constituent.

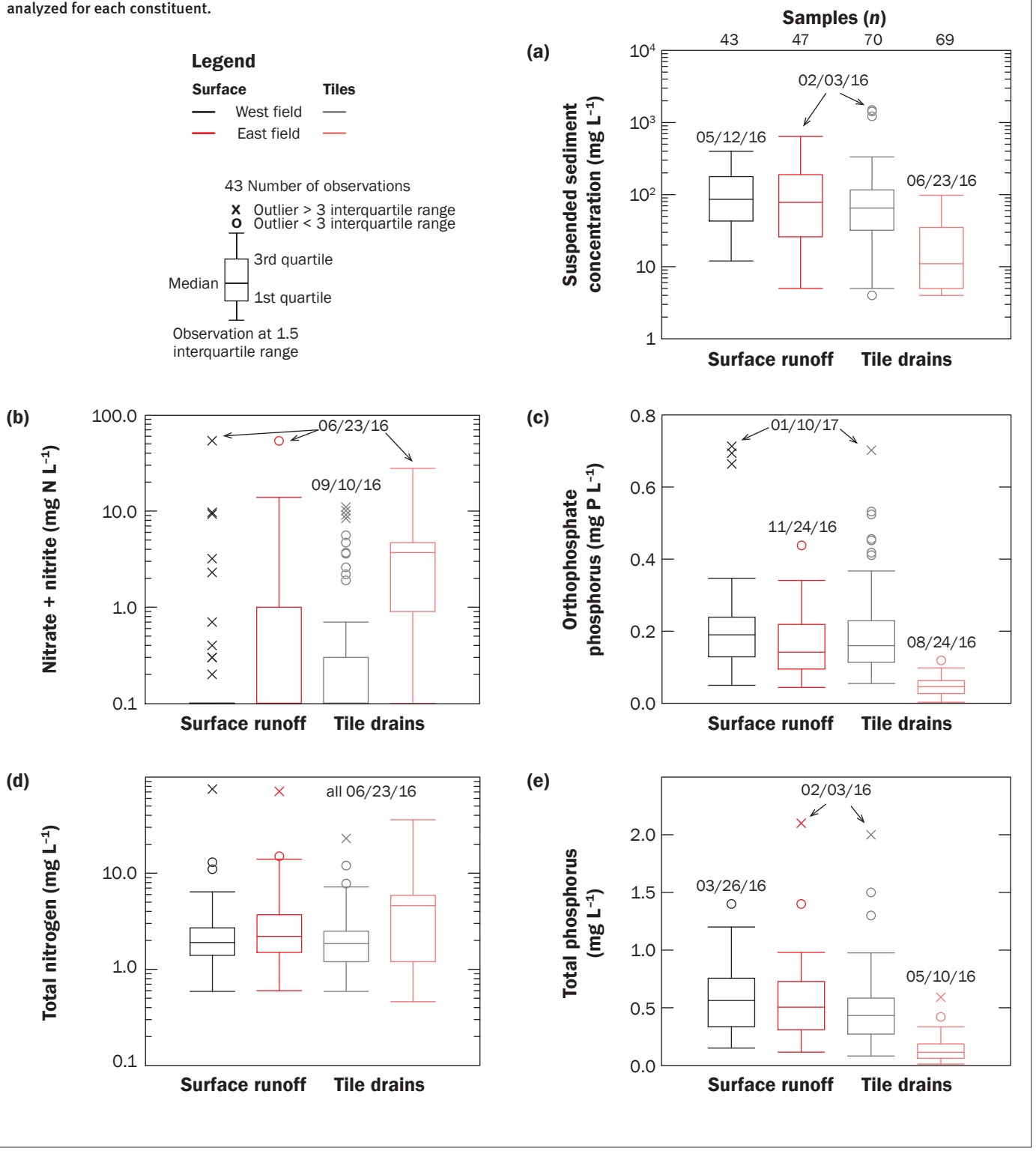

Table 1
US Geological Survey (USGS) monitoring sites.

USGS site ID	Site name
411229084541101	Overland flow east of Bull Rapids Rd near Harlan, Indiana
411229084541102	Drain tile east of Bull Rapids Rd near Harlan, Indiana
411228084541701	Overland flow west of Bull Rapids Rd near Harlan, Indiana
411228084541702	Drain tile west of Bull Rapids Rd near Harlan, Indiana
411228084541703	Meteorological site west of Bull Rapids Rd near Harlan, Indiana

ter frequency) antennae and an incorporated odometer was used to independently locate tile-drain segments; this system was selected because of its successful use in previous investigations (Allred et al. 2004). A NovAtel Inc. (Calgary, Canada) Smart-V1 Global Navigation Satellite System receiver was integrated to geo-reference data; likely tile-drain locations were flagged and later mapped by the farm manager using a real-time kinematic enhanced global positioning system (GPS). During GPR collection, 16 signal traces were averaged at each measurement location, and a measurement was recorded every 0.05 m. Based on time domain reflectometry (Field Scout TDR-300; Spectrum Technologies, Aurora, Illinois), soil-water content in the top 20 cm was 31.6% ($n \approx 30$); the USGS soil-water sensor measured 26.1% at 20 cm depth. An initial soil radar velocity of 0.063 m ns^{-1} was determined based on soil-water content and then used to convert two-way radar travel time to depth values. This initial radar velocity was later refined slightly to 0.066 m ns^{-1} through subsequent computer processing, and depth values were then readjusted accordingly. Depth of investigation was approximately 1.5 m (52 ns of data collected for each signal trace). GPR data were processed using EKKO Project V5 by first applying a signal saturation correction filter in order to remove slowly decaying low-frequency noise introduced by factors related to transmitting and receiving antenna proximity and electrical properties of the ground. Next, a spreading and exponential compensation gain function was utilized to enhance GPR drainage pipe responses. Parameters of the spreading and exponential compensation gain function in this investigation include a starting gain factor of 5.0, an attenuation of 12 decibels m^{-1}, and a maximum gain factor of 1,000. Features recognized in GPR transects were interpreted as either probable tile drain or *other* based on four factors: (1) calculated depth of the pipe (greater than or equal to 0.45 m), (2) appearance of typical GPR pipe responses (reflection hyperbola or banded horizontal features), (3) strength of the GPR pipe response, and (4) adjacent nearby GPR drainage pipe responses that formed a linear trend (features identified in the eastern field were followed as part of each transect). Probable drainage pipe locations met at least criteria 1, 2, and 4 (and almost always 3), while other features might have only met one of the criteria.

Results and Discussion

Water Quantity and Quality. Discharge volumes and water-quality constituents from monitored overland flow and tile drains were compared during the first two years of the study (September 29, 2015, to September 30, 2017).

Differences in the volume and timing of discharge between the western and eastern fields were apparent within the first year of the study and continued through the second year (figure 1). The western tile-drain network had higher peak discharge, and the cumulative discharge was approximately half the total volume recorded from the eastern tile-drain network. The western surface discharge had a maximum 15-minute discharge rate of 1.8 $m^3 s^{-1}$ on May 11, 2016, at 2:30 a.m.; the maximum rate of 1.1 $m^3 s^{-1}$ from the eastern surface discharge occurred 45 minutes later. Each of these were estimated because the berms confining the drainage areas failed as a result of this event. Cumulative surface-runoff discharge during the first two years from the western field was 1,344 $m^3 ha^{-1} y^{-1}$ (averaged over two years and normalized for the entire drainage area) and 1,989 $m^3 ha^{-1} y^{-1}$ from the eastern field; both reached this maximum in the early morning of July 1, 2017. After this date, no additional runoff was recorded through September 30, 2017. For subsurface discharge from the tile-drain networks, the maximum 15 minute discharge rate from the western network was 0.027 $m^3 s^{-1}$ (June 23, 2016) and 0.011 $m^3 s^{-1}$ (December 26, 2016, and May 25, 2017) from the eastern tile network. Cumulative discharge during the first two years from the western tile network was 985 $m^3 ha^{-1} y^{-1}$ (July 12, 2017; normalized for the field area only), ending 11 days after surface runoff ceased for the season. In contrast, total discharge from the eastern field was 1,868 $m^3 ha^{-1} y^{-1}$, with a trickle of drainage (3×10^{-7} $m^3 s^{-1}$) continuing through the end of September 30, 2017. Consequently, although the western tile-drain network had a higher peak discharge, the cumulative discharge was approximately half the total volume recorded from the eastern tile-drain network.

Differences in water quality sample concentrations were also evident in the first two years of the study. Data were compared for the period of record at each site (figure 2). Comparison of the distribution of each water-quality component shows that the western tile-drain network was more similar to surface water from both fields in both concentrations and timing than to the eastern tile-drain network. The western tile-drain network also shared maximum TP and sediment concentration dates with the eastern overland-flow samples. The same June 23, 2016, event was the maximum N from three of four flumes. Both surface flumes exceeded 70 mg L^{-1} TN and 53 mg N L^{-1} NO_3 + nitrite (NO_2), and the tile networks also had maximum TN for this event (23 mg L^{-1} west and 36 mg L^{-1} east). Maximum NO_3 + NO_2 (27.8 mg N L^{-1}) and SSC (98 mg L^{-1}) from the eastern tile were also sampled for the June 23 event. The maximum NO_3 + NO_2 for the western tile (11 mg N L^{-1}) occurred on September 10, 2016—the only maximum date that differed from the eastern surface flume. For example, the maximum TP from the eastern surface flume (2.1 mg L^{-1}) occurred for the same storm event (February 2 to 3, 2016) as that sampled for the western tile-drain network (2 mg L^{-1}); maximum SSC also occurred for this event (640 mg L^{-1} at the eastern surface flume and 1,490 mg L^{-1} for the western tile network). The only maximum that occurred on the same date for the western flumes was PO_4^{3-}—both occurred on January 10, 2017, with the surface concentration (0.713 mg P L^{-1}) similar to that of the tile (0.702 mg P L^{-1}). Maximum PO_4^{3-} for the eastern surface flume (0.438 mg P L^{-1}) occurred on November 24, 2016, and on August 24, 2016, for the eastern tile (0.119 mg P L^{-1}). Maximum TP occurred for the western surface flume on March 26, 2017

(1.4 mg L^{-1}), and on May 10, 2016 (0.591 mg L^{-1}), for the eastern tile.

Multispectral and Thermal Imagery. As a result of differences in water quantity and quality observed at these fields, more information was needed about the tile-drain network. However, neither the owners nor the family currently managing the farm possessed a map of tile drains. Consequently, we turned to remote sensing to provide more information on the location, connectivity, and extent of the tile-drain network.

Multispectral imagery was taken on April 18 and then again on May 10. Thermal-infrared imagery was also taken on May 9 and 10. The first set of imagery had been planned to take advantage of early spring conditions, before plant emergence caused soil-water content to decrease, and to provide detailed orthophotos of the fields, with the secondary goal of learning about the tile-drain network. Prior to these flights, precipitation was last recorded on April 15 (0.25 mm; figure 3), with a total of 52.1 mm in the last 15 days, 47.7 mm of which occurred April 3 through 6. Soil-water content in the top 0.1 m was 18% after reaching a high of 34.2% on April 6; the maximum soil-water content during the period of record was 36.3% (March 14, 2016). We returned 22 days later in response to a large rain event (figure 3); 80.7 mm fell between April 26 and May 5. Soil-water content reached 36% on May 5 and had decreased to 26% by May 9 and 24% by May 10.

Comparison of multispectral imagery from April and May shows that likely tile-drain locations are more evident with a higher soil-water content (figure 4a, 4b, and 4d); this was true whether viewed in the R-G-B or using the NIR-B-G spectrum. There is an indication of individual tiles that join the central tile under the grassed waterway in the western field and clear indication of a tile network in the northern portion of the eastern field. However, the linear features are fuzzy and as much as 11 m wide; these features also seem to discontinue before reaching the eastern tile flume.

Thermal images were collected in May during the late afternoon and morning time periods. Afternoon images were collected during two consecutive days; it was 5.5°C warmer on the afternoon of May 10, when the western field was flown, relative to May 9, when the eastern field was flown; both were clear and sunny. Comparison of thermal-infrared images (figure 4e and 4f) with multispectral images shows that the tile network is better defined, even though the ground resolution is coarser than the multispectral imagery.

The tile-drain network was drawn by hand (figure 4c) using a combination of the May multispectral and thermal images. The tile-drain network in the eastern field shows connectivity between the northern (upstream) and southern (downstream) portions of the field in the thermal imagery, and the network can be followed to the area of the flumes. This link between the upstream and downstream portions of the eastern tile-drain network is an example of a continuous linear feature defined by thermal imagery that could be misinterpreted as the end of

Figure 3
Meteorological data for edge-of-field site. Soil-water content and solar radiation range for the period of record are included for reference; both were near maximum values in the days before the second flight. Note precipitation scale is different.

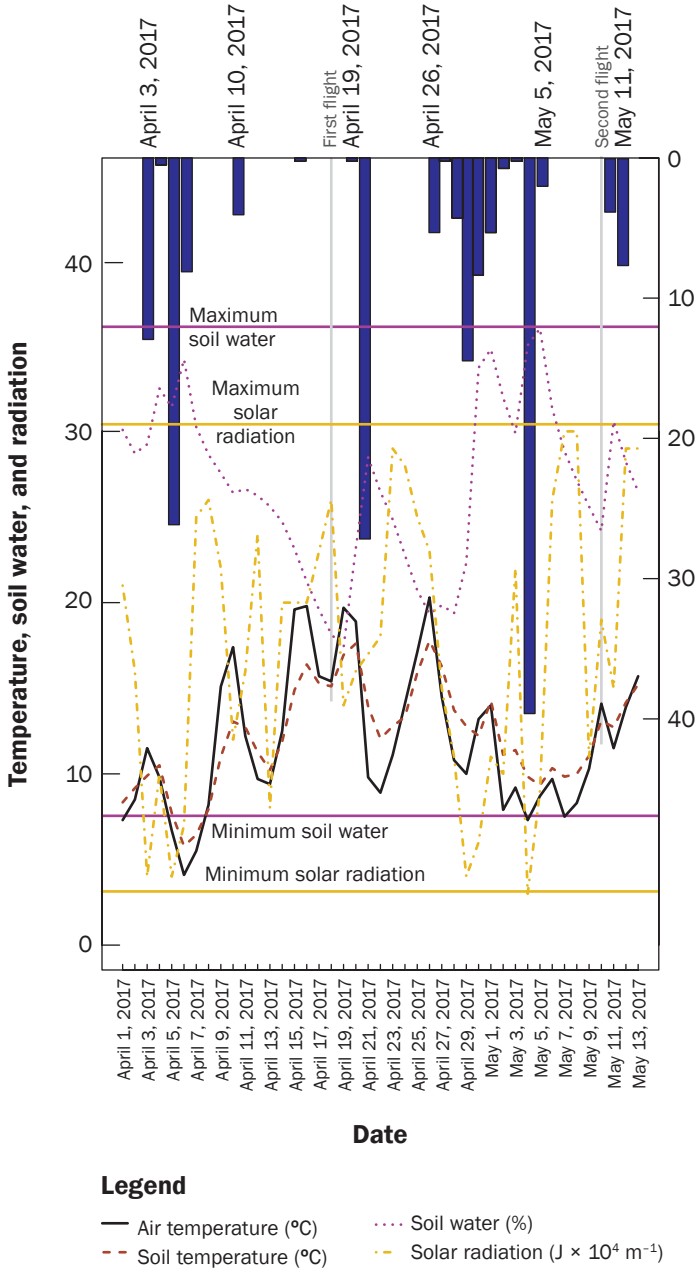

the tile line if only multispectral imagery were available; this could be an indicator of a problem in the tile-drain network. On the western field, the extent of the network can also be better seen in the thermal imagery, including those tiles in the northwestern quadrant, where the network seems to begin. Note that a continuation of these features is also discernable under the grassed waterways.

Using the tile-drain network visible from the thermal images, we investigated the potential connection between the two fields and found a "suckhole" (also known as a "blowout") at the edge of the western field, adjacent to the road (red ellipse in figure 4f). Suckholes are unintended, naturally occurring, open holes that usually develop where a cracked subsurface tile develops a connection to the surface. Trenches were dug in August of 2017 along both sides of the road, and a tile probe was inserted upgradient (northeast) into the cracked tile; however, the tile probe repeatedly stopped, and no tile was found at this location in the eastern field. It seemed that probe was encountering sediment and that there was no open connection under the road.

Ground Penetrating Radar Data. The sampling scheme for the edge-of-field studies requires the paired fields to be separate for both surface and subsurface monitoring, and drainage area must be known in order to normalize the measured sediment and nutrient losses relative to what is applied to the field. Consequently, the northern boundary of the tile networks and the potential for a tile connecting the fields were further investigated using GPR. GPR transects included one south-to-north path along the road on the western field and 10 multidirectional paths on the northern portion of the eastern field. Representative, probable tile-drain segments identified using GPR were distinguished from other subsurface features, including three tiles that were intersected in the western field and multiple continuous tile-drain segments that were followed in the eastern field (figure 5). These GPR transects confirmed (1) the tile-drain network that had been delineated using the thermal imagery and (2) the presence of a tile connecting the eastern and western fields, potentially resulting in 3.2 ha (as drained by approximately 400 m of tile) from the eastern field potentially emptying through the western tile network. A second set of trenches were dug in April of 2018, and the tile drains were found on each side of the road. However, testing with water and dye indicated that there was no direct hydrologic connection between the two fields.

The ability to identify the location of subsurface tile drains has been a research goal for decades because accurately knowing the location of these tiles and being able to readily identify problems in a tile-drain network would enable improved water quality, field management, and cost savings for producers. In addition, accurately assessing contributing drainage areas to individual tile-drain networks is important for understanding how sediment and nutrients are transported from the field to the stream system and how this relates to other agricultural management decisions. This is especially important for research applications, where both surface and subsurface yields are compared—i.e., edge-of-field monitoring sites. If the contributing area of tile systems are inaccurately understood, the primary transport pathways of sediment and nutrients away from the field may be incorrect. This may result in a change (or preservation) of agricultural management that may not have the desired effects.

To our knowledge, this is one of the first comprehensive delineations of a tile-drain network using remote-sensing methods, providing a line network that could be immediately used by the farm manager (Gökkaya et al. 2017). While it is not practical to ground truth the entire tile-drain network depicted in this imagery, some known tile locations were initially used to confirm this interpretation, even without the GPR confirmation. First, there are known tiles below the grassed waterway (intersected by the tile flume) in the western field that are confirmed by the imagery. Second, in the eastern field, the flume was installed to intersect a tile that is in line with the tile-drain network visible extending northeast into the field. Surface erosion in the western field is also evident in these thermal images and can be differentiated from subsurface features because the morning image shows this linear feature as cooler relative to the tile-drain network; this feature is also differentiated in the multispectral images (figure 4).

The thermal imagery provided a more precise location of tile drains than the multispectral imagery, although some segments were only barely discernable in the thermal imagery and may have been overlooked without the multispectral imagery—for example, the northward draining tiles on the eastern field. In addition, some segments in the northeast corner of the eastern field (outside the monitored area) were visible in the imagery but not corroborated by the GPR, perhaps suggesting a different type of subsurface line, like a sump-pump or septic system from a nearby house. Differences in soil type could also contribute to why thermal imagery works better in some areas than in others (Allred et al. 2018). However, the soil map (figure 4c) indicates that tiles are visible in at least five different soils.

The clarity and continuity of the tile network depicted in the thermal imagery suggests that this imagery is less dependent on soil conditions than multispectral imagery. However, this will need to be further tested by collecting imagery under a variety of environmental conditions, including sunlight, soil and air temperatures, soil-water content, and land management. The higher soil-water content in May than in April (24% versus 18%) resulted in much of the tile network being visible in the multispectral imagery, although features were too large (11 m wide) to provide precise locations for the farm manager. Repeat imagery is needed to understand if this large width is a reflection of the number of days since the rainfall event (perhaps demonstrating the effectiveness of tiles to remove water from proximal areas) or the tile spacing (features are more narrow in areas with a higher density of tiles). Additionally, a review of the meteorological data shows that soil-water content changes quickly, making it difficult to target ideal conditions that combine sunny, warmer days with high soil-water content. This is compounded by the spatial variability of soil-water content, which reflects soil characteristics, microtopography, and land management. Ultimately, having both multispectral and thermal imagery was key to creating a complete map of the tile-drain network. This tile-drain network was delineated by hand using the combination of imagery; replication of the method could also involve automated delineation methods.

Tile-drain connectivity to the surface in the western field may explain some differences in water quality between the fields. The development of a surface connection near the road in the western field likely explains why water sampled from the western tile-drain network had a chemical and physical signature more similar to the overland-flow flumes than the eastern tile-drain

Figure 4

Remote-sensing images from April and May of 2017. (a, b, and d) Multispectral images: More linear features are evident in the later red-green-blue (R-G-B)/near infrared-green-blue (NIR-G-B) images, after several rainy days raised the soil-water content. The grassed waterways are visible in each (green in R-G-B and red in NIR). The US Geological Survey (USGS) instruments are visible in the southern third of each image (see 4e). The network visible in the northern part of the eastern field seems to have no connection to the outlet where the tiles are monitored. In addition, some of these linear features are as much as 11 m wide. The gaps in imagery for the April flight are where some flight lines were missed. Ground resolution is approximately 6 cm. The 1 m contour refers to elevation above mean sea level (Indiana Office of Information Technology 2012).

(c) Soil series: Soil series for the site with the linear features that are visible in the remote sensing imagery. Tiles were apparently placed in order to better manage the Pewamo silty clay loam.

(e and f) Thermal infrared images: The tile-drain network is clearly visible in these images, showing connectivity between the northern fields and the outlets to the south. Surface erosion can be discriminated comparing morning and afternoon shots—the erosion feature in the southwest portion of the field is colder than the tile-drain network in the morning, but has a similar thermal signature in the afternoon. Note that the eastern field was imaged the first day, when temperatures were cooler. The red circle shows where the tile was exposed to the surface. Ground resolution is approximately 11 cm. The West and East USGS sites are the collocated surface-runoff and tile-drain flumes. The meteorological site is near the West flumes.

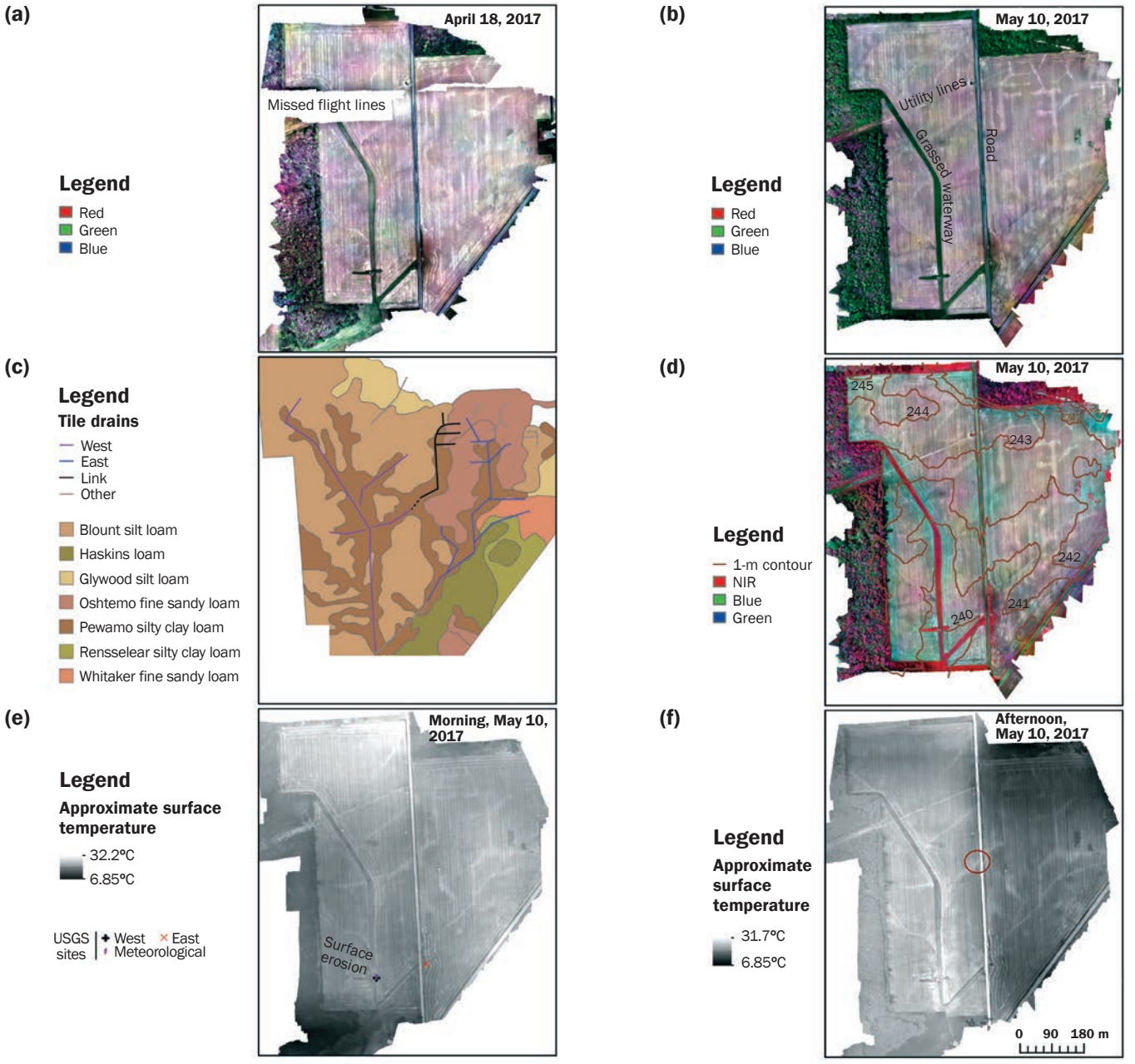

Figure 5

Ground penetrating radar (GPR) responses for probable (a) tile drains (X, Y) and (c) other features (M, N). (b) Thermal image shows location of GPR transects and distribution of features interpreted as tile drains. Examples of GPR responses are shown for comparison and indicated on thermal image (eastern portion of figure 4e). Note the distinct hyperbolas (upside down "U" shape) in X—it is the expected depth (≥0.45 m) and had the same reflection from opposite directions when circled. In other areas (Y), confirmation of a linear feature was done by walking between flags, along the trend of the feature. Interpretation of features as "other" was usually based on poor definition from opposite aspects (M) or shallow depth of feature (N).

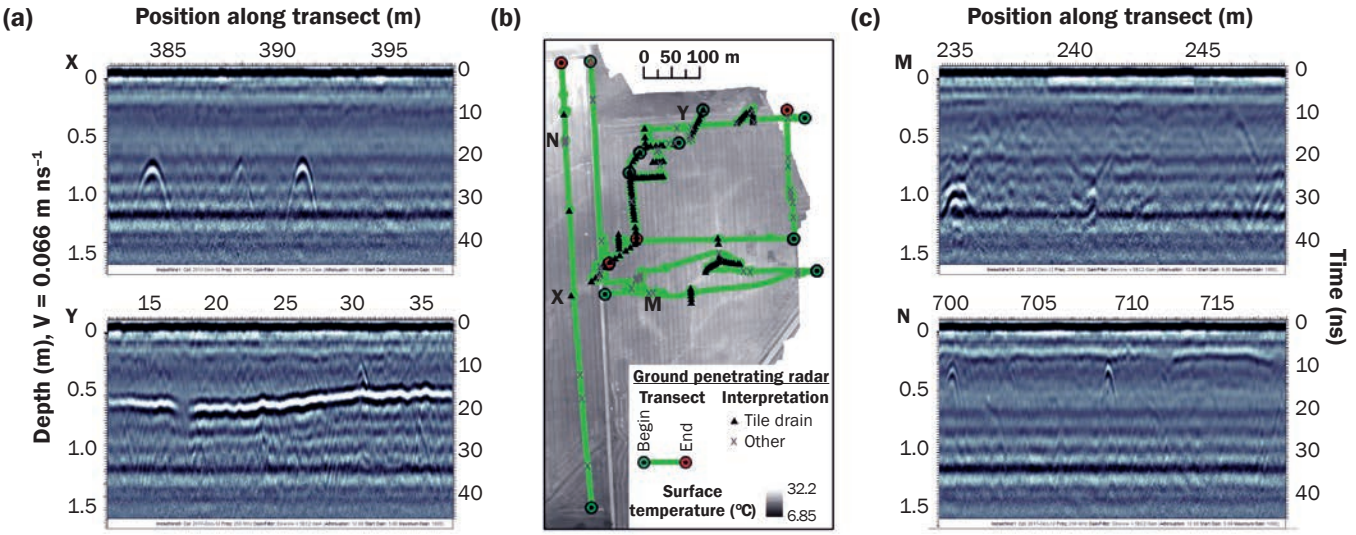

network, specifically the respective concentrations of TP and SSC (figure 2). This may also explain why the peak discharge rate from the western tile-drain network was three times higher than the eastern tile-drain network—runoff from the road and the soil surface was adding to that derived from the more slowly draining soil matrix. In contrast, the eastern field exhibits the more typical tile-drain signature with higher NO_3 concentrations, which is more mobile and easily moves to tile drains, and a longer duration of flow between storms. The higher TN concentrations from the eastern field tile-drain network are because NO_3 is the largest component of TN.

The larger cumulative runoff from the eastern tile-drain network is likely explained by the higher density of tiles in this field, especially where the dendritic (branched) pattern is visible in the northern half. The corollary of this higher tile-drain density in the eastern field is the lower peak discharge and lower cumulative discharge from the surface flume relative to the western surface flume.

The tile-drain network shown in the thermal imagery was used to estimate density (length/area) of subsurface drainage in each field. The total length of visible tile-drain in the eastern field is approximately 1,715 m, compared with only 1,246 m in the western field, 733 m of which is the central tile drain under the grassed waterway. The result is a higher density of tile drains in the eastern field: 115 m ha^{-1} relative to 75 m ha^{-1} in the western field. However, approximately 460 m of tile draining 3.2 ha of the eastern field drains is impeded at the road—likely traveling as a combination of overland flow, soil-matrix flow, and eventually tile-drain flow to the eastern surface and tile flumes. The higher NO_3 concentration in surface runoff from the eastern field may be a consequence of this blocked tile, resulting in water from the tile network exfiltrating and mixing with surface runoff during large events.

A likely explanation of the greater density of tiles in the eastern field is provided by the soils map (figure 4c; USDA NRCS 2016). The Pewamo silty clay is a very deep, very poorly drained soil; the distribution of the tile drains closely follows the distribution of this soil series, suggesting that poor drainage at the surface was likely used to position the network. These same paths are visible in the surface topography (figure 4d), and the tile drains in the northern portion of the eastern field were likely installed to prevent further surface expression of these flow paths. These tiles are a "random" network, meaning that they are not regularly spaced, but instead were placed to take advantage of topographic low points and poorly drained soils in the field. Often, since it is difficult to identify the true location and extent of tile drains within a field or watershed, researchers are forced to assume that low-permeability soils all contain tile drains. This assumption is frequently carried over into hydrologic modeling because there is no better information. However, the high variability of tile installation in these two neighboring fields highlights how inaccurate that can be. It also underscores the importance of high-resolution soil maps to refining estimates of tiles on a regional scale, and that integration of these maps with remote-sensing data could be a method of better mapping tile-drain distribution.

Summary and Conclusions

A combination of thermal and multispectral imagery was used to delineate the tile-drain networks in two adjacent fields. This targeted data collection was a success for two primary reasons. First, while the date of the first flights had been a long-term plan to target general spring conditions after a rain event, it was a smaller rain event than what occurred in May. The second data acquisition was planned for a few days after a large rain event combined with sunny and warm weather. Soil moisture around 25% provided a clearer delineation of tiles using multispec-

tral imagery. Second, the thermal imagery successfully revealed the tile-drain network, and differences between the thermal and multispectral imagery helped identify areas where tile-drain connectivity may be interrupted or less effective. Tiles tended to have warmer temperatures than the surrounding soil, reflecting the lower water content in these locations and relatively rapid response to solar radiation compared to wetter portions of the fields.

Ultimately, rapidly finding and fixing problems in tile-drain networks is the difference between tile drains improving agricultural management versus becoming a rapid path of nutrients and sediment to the stream system. For water quality, tiles exposed to the surface have characteristics similar to surface runoff, specifically higher TP and SSC. In contrast, discharge from tile drains without surface openings is expected to have proportionally larger dissolved forms of N and P.

The outcome of our work was that the landowners were given detailed information that they were able to use to find where the tile-drain network was exposed to the surface; fixing these exposed drains will improve nutrient and water management on their fields. This underscores that tiles with unmanaged/unknown surface connections could be an important source of P and sediment to streams throughout the Midwest. In addition, more differentiation in the research and extension literature of tile networks with managed surface connections from those that are only subterranean could help limit purposeful open surface connections and highlight where incorporating these open connections provides the most benefit.

Identifying discontinuities in the tile-drain network of an individual field is a small step. However, integration of this field-specific imagery with regional approaches that tie field surveys with regional air photos or satellite imagery could provide a new tool to improve basin-wide agricultural management. After further testing and automation, combinations of imagery flown by unmanned aircraft systems—like the quadcopter used here—and other remote-sensing methods could be extended to coordinated delineation of tile drains in critical basins, like the Maumee River and other Great Lakes tributaries, in order to decrease nutrient transport to streams and water bodies while better protecting agricultural fields and improving crop yields.

Acknowledgements

This work was partially supported by the Great Lakes Restoration Initiative. We appreciate the ongoing cooperation of the Allen County Soil Water Conservation District and the landowners and managers who have allowed monitoring on their property.

Disclaimer

Any use of trade, firm, or product names is for descriptive purposes only and does not imply endorsement by the US Government.

References

Allred, B., N. Eash, R. Freeland, L. Martinez, and D. Wishart. 2018. Effective and efficient agricultural drainage pipe mapping with UAS thermal infrared imagery: A case study. Agricultural Water Management 197:132-137.

Allred, B.J., N.R. Fausey, J.L. Peters, C. Chen, J.J. Daniels, and H.Youn. 2004. Detection of buried agricultural drainage pipe with geophysical methods. Applied Engineering in Agriculture 20(3):307.

Baker, N.T., W.W. Stone, J.T. Wilson, and M.T. Meyer. 2006. Occurrence and transport of agricultural chemicals in Leary Weber Ditch basin, Hancock County, Indiana, 2003-04. Scientific Investigations Report 50. Reston, VA: US Geological Survey.

Capel, P.D., D.M. Wolock, R.H. Coupe, and J.L. Roth. 2018. A conceptual framework for effectively anticipating water-quality changes resulting from changes in agricultural activities. Scientific Investigations Report. Reston,VA: US Geological Survey.

Cuadra, P.E., and P. Vidon. 2011. Storm nitrogen dynamics in tile-drain flow in the US Midwest. Biogeochemistry 104(1):293-308.

Fausey, N.R., L.C. Brown, H.W. Belcher, and R.S. Kanwar. 1995. Drainage and water quality in Great Lakes and Cornbelt states. Journal of Irrigation and Drainage Engineering 121(4):283-288.

Gentry, L.E., M.B. David, T.V. Royer, C.A. Mitchell, and K.M. Starks. 2007. Phosphorus transport pathways to streams in tile-drained agricultural watersheds. Journal of Environmental Quality 36(2):408-415.

Gökkaya, K., M. Budhathoki, S.F. Christopher, B.R. Hanrahan, and J.L. Tank. 2017. Subsurface tile drained area detection using GIS and remote sensing in an agricultural watershed. Ecological Engineering 108:370-379.

Hirsch, R., L. DeCicco, D. Lorenz, J. Read, L. Carr, and D. Watkins. 2017. dataRetrieval - Retrieval functions for USGS and EPA hydrologic and water Quality data. 2.6.7. https://github.com/USGS-R/dataRetrieval.

Ho, J.C., and A.M. Michalak. 2015. Challenges in tracking harmful algal blooms: A synthesis of evidence from Lake Erie. Journal of Great Lakes Research 41(2):317-325.

Homer, C.H., J.A. Fry, and C.A. Barnes. 2012. The National Land Cover Database. US Geological Survey Fact Sheet. Reston,VA: US Geological Survey.

IDEM (Indiana Department of Environmental Management). 2016. Appendix P: Finalized 2016 303(D) List of Impaired Waters [XLS]. Water Quality Assessments and Reporting. Indianapolis, IN: Indiana Department of Environmental Management. https://in.gov/idem/nps/2647.htm.

Indiana Office of Information Technology. 2012. Indiana Statewide Imagery and LiDAR Program - 1-ft pixel. Indianapolis, IN: Indiana Office of Information Technology. www.indianamap.org.

Lorenz, D. 2015. smwrGraphs - Graphing Functions. 1.1.1. https://github.com/USGS-R/.

Maccoux, M.J., A. Dove, S.M. Backus, and D.M. Dolan. 2016. Total and soluble reactive phosphorus loadings to Lake Erie: A detailed accounting by year, basin, country, and tributary. Journal of Great Lakes Research 42(6):1151-1165.

MicaSense Inc. 2015. MicaSense RedEdge. I. Seattle, WA: MicaSense.

Naz, B.S., S. Ale, and L.C. Bowling. 2009. Detecting subsurface drainage systems and estimating drain spacing in intensively managed agricultural landscapes. Agricultural Water Management 96(4):627-637.

PIX4D. 2018. Thermal Projects FAQ. https://support.pix4d.com/hc/en-us/articles/360000173463-Processing-thermal-images#label3.

R Core Team. 2014. R: A language and environment for statistical computing. R Foundation for Statistical Computing. Vienna, Austria: The R Foundation for Statistical Computing. http://www.R-project.org/.

Robertson, D.M., and D.A. Saad. 2011. Nutrient inputs to the Laurentian Great Lakes by source and watershed estimated using SPARROW watershed models. Journal of the American Water Resources Association 47(5):1011-1033.

Smith, D.R., K.W. King, L. Johnson, W. Francesconi, P. Richards, D. Baker, and A.N. Sharpley. 2015. Surface runoff and tile drainage transport of phosphorus in the midwestern United States. Journal of Environmental Quality 44(2):495-502.

Stuntebeck, T.D., M.J. Komiskey, D.W. Owens, and D.W. Hall. 2008. Methods of data collection, sample processing, and data analysis for edge-of-field, streamgaging, subsurface-tile, and meteorological stations at discovery farms and pioneer farm in Wisconsin, 2001-7. USGS 2008-1015. Open-File Report. Middleton, WI: US Geological Survey, Wisconsin Water Science Center.

Stuntebeck, T.D., M.J. Komiskey, M.C. Peppler, D.W. Owens, and D.R. Frame. 2011. Precipitation-runoff relations and water-quality characteristics at edge-of-field stations, Discovery Farms and Pioneer Farm, Wisconsin, 2003-8. Scientific Investigations Report. Reston, VA: US Geological Survey.

USDA NRCS (Natural Resources Conservation Service). 2016. Soil Survey Geographic (SSURGO) Database for Allen County, IN. Washington, DC: USDA Natural

Resources Conservation Service. https://websoilsurvey.sc.egov.usda.gov/App/WebSoilSurvey.aspx.

USEPA (Environmental Protection Agency). 1972. Federal Water Pollution Control Act (Clean Water Act. US Environmental Protection Agency (USEPA), 33 U.S.C. §1251 et seq. (1972). Washington, DC: USEPA.

USGS (US Geological Survey). 2016. GLRI Edge-of-Field Monitoring. Washington, DC: US Geological Survey. https://wim.usgs.gov/geonarrative/glri-eof/.

USGS. 2017. National Water Information System—Web interface (NWIS). Washington, DC: US Geological Survey. https://dx.doi.org/10.5066/F7P55KJN.

Vidon, P., and P.E. Cuadra. 2010. Impact of precipitation characteristics on soil hydrology in tile-drained landscapes. Hydrological Processes 24(13):1821-1833.

Williamson, T.N., and S.M. Meyer. 2018. Low-altitude multispectral and thermal-infrared imagery from agricultural fields, Black Creek basin, Allen County, IN—spring 2017. Data Release. Washington, DC: US Geological Survey. https://doi.org/10.5066/F7Q81C9V.

Zambrano-Bigiarini, M. 2017. hydroTSM - Time series management, analysis, and interpolation for hydrological modelling. Version 0.5-1. https://github.com/hzambran/hydroTSM.

Zucker, L.A., and L.C. Brown. 1998. Agricultural drainage: Water quality impacts and subsurface drainage studies in the Midwest. Extension Bulletin. Ohio State University 871: 40. Columbus, OH: The Ohio State University.